Editors' Suggestion

Measurement of the Alfvén Wave Parametric Decay Instability Growth Rate

S. Dorfman,[1,2] F. Li,[3] X. Fu,[4,3] S. Vincena,[1] P. Pribyl,[1] and T. A. Carter[1,5]
[1]University of California Los Angeles, Los Angeles, California 90095, USA
[2]Space Science Institute, Boulder, Colorado 80301, USA
[3]New Mexico Consortium, Los Alamos, New Mexico 87544, USA
[4]Los Alamos National Laboratory, Los Alamos, New Mexico 87545, USA
[5]Oak Ridge National Laboratory, Oak Ridge, Tennessee 37831, USA

(Received 5 November 2025; accepted 9 February 2026; published 31 March 2026)

Alfvén waves, a fundamental mode of magnetized plasmas, are ubiquitous in space and laboratory plasmas. The nonlinear behavior of these modes is thought to play a key role in important problems in space plasma, such as the heating of the solar corona and solar wind turbulence. In particular, theoretical predictions show that these Alfvén waves may be unstable to various parametric instabilities, but space observations of these processes are limited. We demonstrate the first measurement of the Alfvén wave parametric decay instability (PDI) growth rate. Experiments are conducted on the Large Plasma Device at UCLA in which a high amplitude $\delta B/B_0 \sim 0.7\%$ pump Alfvén wave is launched from one end of the device and a smaller seed Alfvén wave is launched from the other side. When the frequency of the seed wave is chosen to match the backward wave expected from PDI, damping of the seed wave is reduced. We compare this reduction in damping to the theoretically expected PDI growth rate while accounting for acoustic mode damping. Results show agreement between measurements and theoretical predictions. This not only provides critical validation for PDI theories and simulations that could help interpret future space observations but also suggests a new way of studying similar nonlinear wave phenomena.

DOI: 10.1103/qc7s-scbk

Alfvén waves, a fundamental mode of magnetized plasmas, are ubiquitous in space and laboratory plasmas. The nonlinear behavior of these modes is thought to play a key role in important problems such as the heating of the solar corona [1], the generation of solar wind turbulence [2–4], and the loss of energetic particles in tokamaks [5]. A large body of theoretical work (e.g., [6–13]) shows that Alfvén waves may be unstable to various parametric instabilities, with the parametric decay instability (PDI) being the most common. In PDI, a large-amplitude pump Alfvén wave will decay into a forward-propagating ion acoustic wave and a backward-propagating Alfvén wave. The acoustic mode is driven by a parallel (to the mean magnetic field) ponderomotive force produced due to the coupling of the two Alfvén waves; in other words, compressible effects are critical.

Alfvén wave PDI may be important in a variety of contexts, but observational evidence is very limited. For example, if a large-amplitude Alfvén wave propagating up from the photosphere to the corona undergoes PDI, the resulting acoustic mode could directly heat ions, contributing to coronal heating [14]. Although observations in the lower solar atmosphere show a relationship between density and velocity fluctuations that is indicative of PDI [15], it is not clear whether the reported acoustic waves carry enough energy flux to heat the plasma [16]. In the solar wind, Alfvénic modes move outward from their source at the Sun; PDI is therefore a possible source of backward-propagating Alfvén waves that could seed solar wind turbulence [17]. Spacecraft observations show that the PDI growth rate limits the solar wind parameter space, suggesting that the instability is present [18]. However, attempts at direct observation (conducted in Earth's ion foreshock) have been inconclusive [19–21]. There is therefore an important opening for controlled laboratory experiments to validate the theoretical predictions and connect with the spacecraft measurements.

Extensive prior work on Alfvén waves has been conducted on the Large Plasma Device (LAPD) at UCLA. This work first focused on the properties of linear Alfvén waves [22–25], which was followed by studies of nonlinear properties. In the later set of experiments, two launched Alfvén waves nonlinearly interact to drive a nonresonant mode [26], a drift wave [27], an acoustic mode [28,29], or an Alfvén mode [30]. However, attempts to observe PDI using a single large-amplitude Alfvén wave were not successful; a modulational-like instability driven by perpendicular nonlinear terms was observed instead [31]. Subsequent theoretical and simulation work revealed that direct observation of PDI is challenging in LAPD due to damping of the three waves involved [32]. To mitigate this difficulty, we proposed a new scheme to measure the PDI growth rate by launching both the large-amplitude pump and a small-amplitude seed wave, with the latter tuned to the

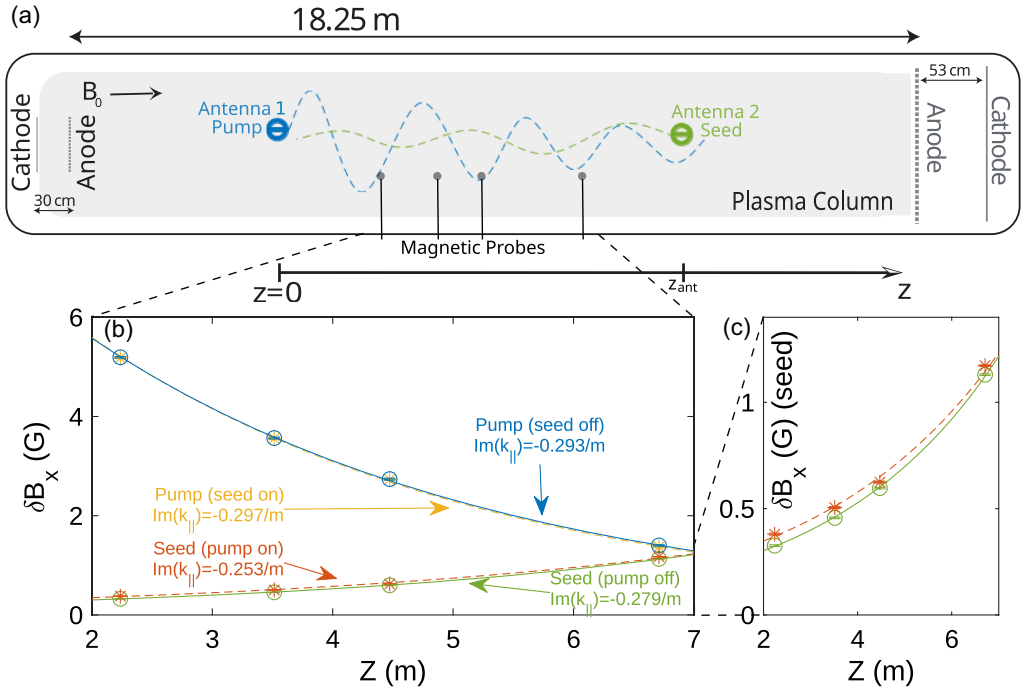

FIG. 1. Experimental setup in the Large Plasma Device. (a) Antenna launch a large-amplitude pump wave from $z = 0$ and a small-amplitude seed wave from $z = z_{\mathrm{ant}} = 8.95$ m; the seed is matched to the expected PDI backward wave. Probes placed in the plasma detect changes in the amplitude of the seed wave in the presence of the pump. (b) Amplitude of the 173 kHz pump and 162.25 kHz seed at the center of the antenna pattern in the transverse x-y plane as a function of axial location z. Solid curves represent cases with only a single wave on, while dashed curves represent cases with both waves on. (c) Blowup of the seed wave amplitude profile to show a clear reduction in damping with the pump present.

frequency of the PDI backward wave. By comparing the seed wave amplitude with the pump on to the seed wave amplitude with the pump off, it is possible to isolate the PDI contribution [33]. The present Letter, which demonstrates the first measurement of the Alfvén wave PDI growth rate, is the experimental realization of this scheme.

Experiments are conducted using the LAPD at UCLA, a cylindrical vessel capable of producing an 18.25 m long, quiescent, magnetized plasma column for wave studies. The plasma is produced by a pair of lanthanum hexaboride (LaB_6) cathodes, as shown in Fig. 1(a): the larger diameter cathode [34] on the right discharges over ~12 ms, ionizing gas puffed near the close-by anode; the smaller diameter cathode [35] on the left is on for the final ~10 ms to minimize transverse density variation in the shadow of antennas placed in the plasma column. Data are taken during ~2 ms of the several milliseconds when both discharge circuits display a current flattop. Plasma parameters for the present Letter are $n_e = 3.3 \pm 0.1 \times 10^{12}$ cm^{-3}, $T_e = 4.9 \pm 0.4$ eV, and $B_0 = 770$ G in the z direction ($\beta_e = 0.0011$) with a fill gas of helium.

As illustrated in Fig. 1(a), one antenna is placed at each end of the LAPD to launch both forward and backward Alfvén waves. Magnetic and Langmuir probes placed between the antennas detect the signatures of the launched Alfvén and generated ion acoustic modes. The antennas are rotating magnetic field antennas described in Gigliotti *et al.* [36] with two current loops, oriented so that each loop has a dipole moment in one of the two directions (x and y) transverse to the background magnetic field. For the purposes of the present experiment, only the loop that predominantly produces B_x is driven on each antenna. A similar two-antenna experimental setup was previously used to validate the three wave coupling at the heart of PDI; these experiments verified that an acoustic mode resonance appears in the beat wave response with the expected frequency and wave number matching relations [28,29]. In the new experiments reported here, the backward wave launched from $z = z_{\mathrm{ant}} = 8.95$ m is a small-amplitude seed wave. The large-amplitude forward pump wave is launched from $z = 0$; this pump wave will be turned on and off between discharges to isolate the contribution of PDI to the amplitude of the seed wave, as proposed by the scheme of Li *et al.* [33].

Figures 1(b) and 1(c) show the amplitudes of the pump and seed waves as they propagate from their respective antennas. The amplitude profiles are fitted to exponential functions with the corresponding spatial damping rate [$\mathrm{Im}(k_\parallel)$] given in the figure. For our chosen experimental parameters, damping is due to a mix of electron Landau damping, ion-electron collisional damping, and geometric attenuation of the Alfvén wave cone [32,37–40]. Note from

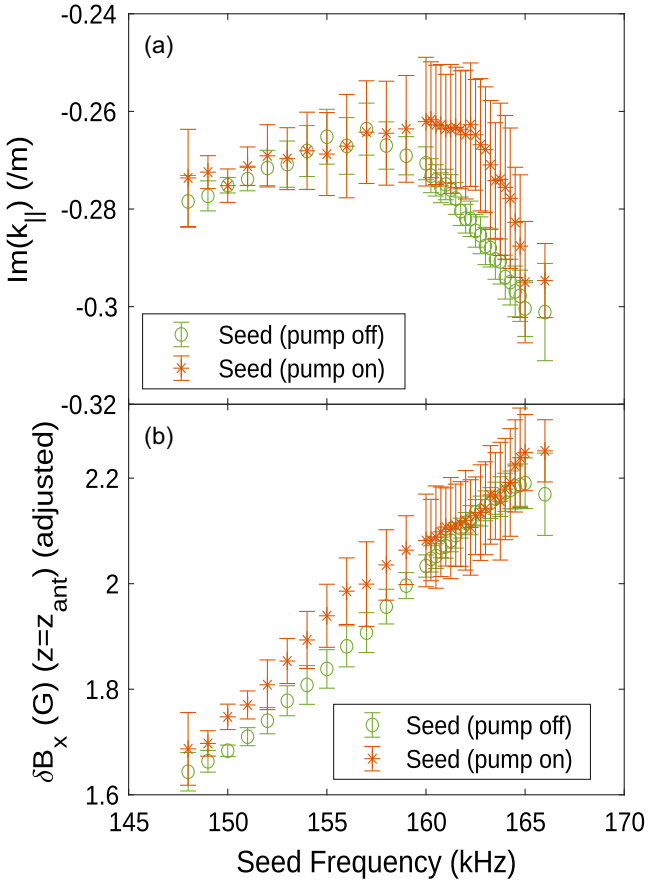

FIG. 2. (a) Spatial damping rate of the seed wave and (b) extrapolated wave amplitude at $z = z_{\mathrm{ant}} = 8.95$ m. Both quantities are calculated from exponential fits of the axial profile of seed wave amplitude. Data are from a scan of the seed frequency with seed wave magnetic field amplitude measured at the same four z locations used in Figs. 1(b) and 1(c). The wave amplitude plotted in (b) is adjusted to account for variations in the antenna current; this is done by scaling all fields to the values expected for the measured antenna current at 162.5 kHz.

Fig. 1(b) that the large pump wave is barely affected by the small-amplitude seed; the pump retains the same amplitude profile and damping rate when the seed is turned on. By contrast, the blowup [Fig. 1(c)] shows that there is a clear reduction in the damping of the seed wave when the pump is turned on.

This reduction in damping should only occur when the seed wave frequency is tuned to match the backward wave predicted from PDI. We therefore repeat the analysis in Fig. 1(c) for different seed wave frequencies and plot the exponential fit coefficients in Fig. 2. Figure 2(a) compares seed wave damping rates with only the seed on and seed wave damping rates with both the pump and seed on. For some frequencies (most notably from 148 to 158 kHz in the left half of the range), there is little difference between the pump-on and pump-off cases. However, near 163 kHz, there is a clear difference outside of the error bar. As we shall see later in this Letter, it is in this frequency range that a finite PDI growth rate is expected. Results in Fig. 2(a) also suggest that pump effects that may uniformly reduce seed wave damping for all seed frequencies (e.g., heating of the plasma by the large-amplitude pump) are not important in this dataset.

The presence of the pump wave also affects the seed antenna coupling (i.e., the wave amplitude produced at a given frequency and antenna current), as shown in Fig. 2(b). The Appendix discusses how we isolate this difference from the effect of PDI growth.

We next compare the measured reduction in seed wave damping to theoretical predictions for PDI growth. Per Li *et al.* [33], the effective PDI growth rate is given by

$$\gamma_g^{\mathrm{eff}} = \frac{1}{2}\left(-\Gamma_s + \sqrt{\Gamma_s^2 + 4\gamma_g^2}\right), \tag{1a}$$

$$\gamma_g = \frac{\omega_1}{2}\frac{\delta B_1}{B_0}\frac{1}{\beta^{1/4}}. \tag{1b}$$

Here, γ_g is the PDI growth rate for a single, large-amplitude, $k_\perp = 0$ Alfvén wave with frequency ω_1 in the absence of secondary wave damping. The effective growth rate γ_g^{eff} takes into account acoustic damping at a rate given by Γ_s, discussed below. Note that γ_g^{eff} will always be greater than zero, confirming the thresholdless nature of our scheme. Damping of the seed wave is not included in this expression because the seed wave is continuously driven for 200+ cycles, leading to a steady-state (constant) seed amplitude at any given spatial location.

A graphical representation of the theoretical growth rate as a function of axial location is shown in Fig. 3. Here, we use the two-fluid theory of Wong and Goldstein [9] and Hollweg [12]; because of the finite value of $\omega_1/\omega_{ci} = 0.59$ used for the pump wave, the result plotted is ~10% smaller than Eq. (1b). Per Eq. (1b), the variation in the growth rate with axial location (dash-dotted yellow) follows the spatial trend of the pump wave amplitude (thick blue) such that the two curves exactly overlap in Fig. 3.

To evaluate the effective growth rate, it is first necessary to determine the acoustic mode damping rate Γ_s. Acoustic mode damping results from a combination of ion-neutral collisional damping and ion Landau damping. Both damping rates are related to the helium ion temperature, which is not directly measured in the present experiment. Instead, we apply the method of Dorfman and Carter [28] to determine the acoustic mode phase speed and use the result to constrain the ion temperature. At an acoustic mode frequency of 10.5 kHz, corresponding to the experimentally measured resonance (Fig. S2 of Supplemental Material [41]), magnetic probe measurement of the launched Alfvén waves and three wave matching conditions yield an expected parallel wave number for the acoustic mode of 5.4 ± 0.2 /m. The resulting acoustic mode phase speed of 12.1 ± 0.5 km/s is only slightly larger than the sound speed

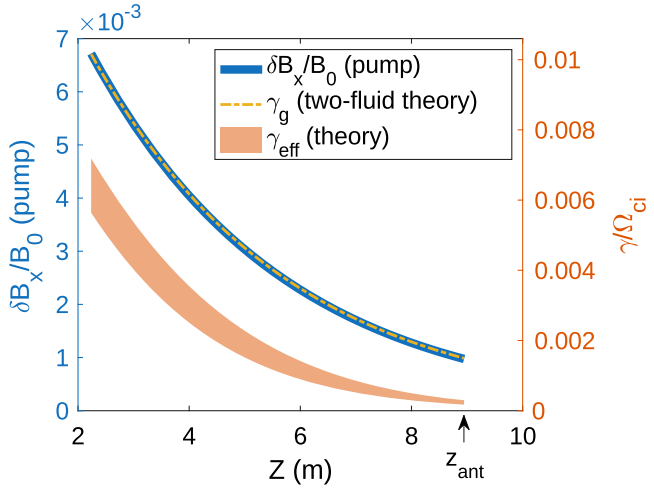

FIG. 3. Amplitude profile of the pump wave (thick blue), PDI growth rate from the two-fluid theory of Wong and Goldstein [9], Hollweg [12] (dash-dotted yellow), and theoretical PDI growth rate after accounting for acoustic wave damping (shaded red). The width of the γ_{eff} curve arises from experimental uncertainty in the ion temperature.

$C_s = \sqrt{T_e/m_i} = 10.8 \pm 0.4$ km/s, which according to the kinetic dispersion relation of Hasegawa and Chen [7] is consistent with ion temperatures of $T_i = 0.5 \pm 0.3$ eV.

With this ion temperature estimate in place, we estimate the ion-neutral collision frequency (ν_{in}) as 33 ± 8 kHz. We use a collisional cross section of $\sim 10^{-14}$ cm^2 calculated by Barata and Conde [42], Swaczyna *et al.* [43], and Eq. (25) of Ballester *et al.* [44] for the ion-neutral collision rate. This contributes $\nu_{\mathrm{in}}/2$ to the acoustic mode temporal damping rate. The factor of 2 arises from the solution of the acoustic wave dispersion relation obtained from the continuity and ion momentum equations [28,45] with complex ω and real k. For our calculated ion-to-electron temperature ratio ($\sim$0.1), the Landau damping rate contribution will be more than a factor of 5 smaller. Both ion-neutral collisions and ion Landau damping are used to calculate Γ_s. Per Eq. (1a), this yields the shaded red region in Fig. 3 for γ_{eff}, with the error bar due to the uncertainty in the inferred ion temperature.

Comparison of the resulting effective growth rate with experimental measurements requires knowledge of how the growth rate will contribute to the wave amplitudes measured at a given spatial point. To do this, we use Eq. (3) of Li *et al.* [33] and convert the sum over bins to an integral over space to write an expression for the convective growth of the seed wave due to PDI,

$$\frac{\delta B_{x,\mathrm{on}}}{\delta B_{x,\mathrm{off}}} = \exp\left(\int_z^{z_{\mathrm{ant}}} \frac{\gamma^{\mathrm{eff}}(z')}{v_{\mathrm{gr}}} dz'\right). \tag{2}$$

Here, $\delta B_{x,\mathrm{on}}$ is the amplitude of the seed wave with the pump on, $\delta B_{x,\mathrm{off}}$ is the amplitude of the seed wave with the pump off, and v_{gr} is the group velocity of the seed wave calculated from the dispersion relation. $\gamma^{\mathrm{eff}}/v_{\mathrm{gr}}$ is then the convective growth rate, which is a function of z due to the pump wave amplitude profile (Fig. 3). We integrate this growth rate over the region between the seed antenna location z_{ant} (marked in Fig. 3) and the measurement location z (where $z < z_{\mathrm{ant}}$) to find the reduction in wave damping that can be attributed to PDI. Note that the resulting expression for $\delta B_{x,\mathrm{on}}/\delta B_{x,\mathrm{off}}$ is not simply an exponential function of z; this contributes to the error in the exponential fit in the "Seed (pump on)" case at frequencies with a PDI contribution in Fig. 2.

To remove this source of error, we plot $\delta B_{x,\mathrm{on}}/\delta B_{x,\mathrm{off}}$ directly in Fig. 4 and compare to the theoretical results of Eq. (2). Each panel of Fig. 4 plots the seed wave amplitude ratio at a different axial location, with Fig. 4(a) being closest to the pump antenna and Fig. 4(c) closest to the seed antenna. Each point in Fig. 4 has been divided by 1.039 ± 0.035 in order to remove the antenna coupling effect discussed in the Appendix.

The experimental data points in Fig. 4 show that the measured seed wave amplitude is enhanced in the presence of the pump wave at frequencies between 160 and 165 kHz at small z, i.e., when the seed wave has propagated a considerable distance toward the pump antenna. The data points showing this enhancement in Figs. 4(a) and 4(b) have error bars well above the horizontal dashed line representing no change, indicating clear experimental identification of the PDI contribution. The shaded regions show the corresponding theoretical predictions from Eq. (2), which are constructed using the two-fluid theory of Wong and Goldstein [9] and Hollweg [12], together with Eq. (1a) to determine γ_{eff} at each frequency and z location. The width of the shaded regions is due to the uncertainty in our inferred ion temperature. At all three z locations, the peak seed wave amplitude enhancement predicted by theory falls largely within the error bar of the experimental measurement, which represents the first measurement of the Alfvén wave PDI growth rate.

Note that the shaded theory curves in Fig. 4 assume a $k_\perp = 0$ right-hand circularly polarized pump, but the pump wave in the experiment is linearly polarized with $k_\perp \rho_s \sim 0.22$. This discrepancy is due to the fact that the theory of Wong and Goldstein [9] and Hollweg [12] is only valid for a circularly polarized, $k_\perp = 0$ pump with dispersion relation $\omega = k_\parallel V_A \sqrt{1 \pm \omega/\Omega_i}$ (here, $+$ corresponds to right-hand polarization and $-$ corresponds to left-hand polarization). Per the calculation leading to Eq. (1) of Dorfman and Carter [29], variation in the Alfvén dispersion relation will shift the predicted resonant acoustic mode frequency. Since the actual Alfvén wave launched in our LAPD experiment is linearly polarized, it makes more physical sense to use a dispersion relation similar to Gekelman *et al.* [46] and Hollweg [47]: $\omega = k_\parallel V_A \sqrt{1 + (k_\perp \rho_s)^2 - (\omega/\Omega_i)^2}$. While to the authors'

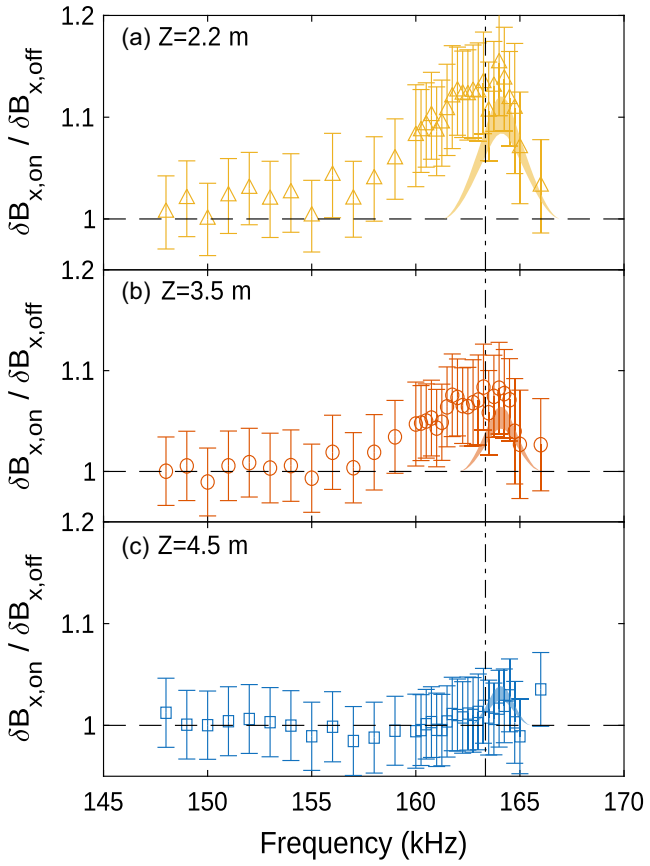

FIG. 4. Enhancement in the seed wave magnetic field amplitude due to PDI at three different z locations. Panels (a)–(c) show axial locations in the order of decreasing seed wave propagation distance, with (a) being farthest from the seed wave antenna. Data points in each panel show the measured enhancement, the shaded curves show the theoretical predictions obtained by integrating the convective growth rate for a right-hand polarized $k_\perp = 0$ pump, and the vertical dash-dotted line indicates the expected location of the growth rate peak for a linearly polarized pump with $k_\perp \rho_s = 0.22$.

knowledge there is no derivation of PDI that uses this dispersion relation, we can use the method of Dorfman and Carter [29] to estimate the acoustic mode resonance at 9.7 kHz. This corresponds to a seed frequency of 163 kHz and is marked by the vertical dash-dotted line in Fig. 4. This line matches the peak in Fig. 4 and is close to the peak in fluctuating ion saturation current at an acoustic mode frequency of 10.5 kHz (Fig. S2 of Supplemental Material [41]). Note that the key difference in the dispersion relation derived assuming a linearly polarized pump is the square on the $\omega/\Omega_i = 0.59$ factor; the perpendicular wave number normalized to the ion sound gyroradius $k_\perp \rho_s \sim 0.22$ is comparatively insignificant.

Therefore, we have demonstrated the first measurement of the Alfvén wave PDI growth rate in the laboratory. Because of wave damping, the direct observation of PDI is challenging under currently achievable laboratory plasma conditions [32]; the new technique demonstrated in this Letter overcomes this critical problem by isolating the contribution of PDI to the amplitude of a small seed wave. Both the reduction in seed wave damping due to PDI and the resonant peak in this response match theoretical predictions.

This proof-of-principle measurement opens a new avenue for validation of Alfvén wave PDI theory and simulation; these validated tools can then provide critical insight for the interpretation of spacecraft measurements where PDI may be active. More broadly, the method newly demonstrated in this Letter may be used to validate theoretical predictions and confirm growth rates for a general class of nonlinear phenomena involving parametric excitation of coupled waves [48]. Our results therefore suggest an entirely new method of studying this class of nonlinear wave phenomena in fields from plasma physics [7,49] to nonlinear optics [50–53] to fluid mechanics [54].

To enhance this novel experimental platform, we next aim to expand our measurement to additional cases. This will include conducting routine ion temperature measurement using an available Doppler line broadening diagnostic to enable more accurate estimation of acoustic damping rates. In recent related simulation work [33], we also found that, when the pump wave is on, the seed wave may be reflected at the location of the pump antenna. We verified that this is a negligible effect in the present Letter by carefully examining the seed wave amplitude profile off resonance with the pump on (Fig. S3 of Supplemental Material [41]). However, preliminary data from other experimental cases suggest significant reflection; this could be caused by local modification of the plasma and/or field profile at the pump injection location and will be the subject of a future publication.

Acknowledgments—The authors thank S. K. P. Tripathi for insightful discussions and assistance with the experiment and Z. Lucky, M. Drandell, T. Ly, R. Buckley, and T. Sketchley for their excellent technical support. This work was supported by the DOE (Grants No. DE-SC0023893 and No. DE-SC0025443) and NASA (Grant No. 80NSSC23K0695). X. F. acknowledges support from NASA (Grant No. 80NSSC23K0101) and NSF (Grant No. 2229101). This work was performed at the UCLA Basic Plasma Science Facility, which is supported by the DOE and NSF.

Data availability—The data that support the findings of this article are openly available [55].

[1] D. B. Jess, M. Mathioudakis, R. Erdélyi, P. J. Crockett, F. P. Keenan, and D. J. Christian, Alfvén waves in the lower solar atmosphere, Science **323**, 1582 (2009).

[2] D. Verscharen, K. G. Klein, and B. A. Maruca, The multi-scale nature of the solar wind, Living Rev. Solar Phys. **16**, 5 (2019).

[3] W. H. Matthaeus, Turbulence in space plasmas: Who needs it?, Phys. Plasmas **28**, 032306 (2021).

[4] A. A. Schekochihin, MHD turbulence: A biased review, J. Plasma Phys. **88**, 155880501 (2022).

[5] W. W. Heidbrink, Basic physics of Alfvén instabilities driven by energetic particles in toroidally confined plasmas, Phys. Plasmas **15**, 055501 (2008).

[6] R. Z. Sagdeev and A. Galeev, *Nonlinear Plasma Theory*, Frontiers in Physics (W. A. Benjamin, New York, 1969).

[7] A. Hasegawa and L. Chen, Kinetic processes in plasma heating by resonant mode conversion of Alfvén wave, Phys. Fluids **19**, 1924 (1976).

[8] M. L. Goldstein, An instability of finite amplitude circularly polarized Alfvén waves, Astrophys. J. **219**, 700 (1978).

[9] H. K. Wong and M. L. Goldstein, Parametric instabilities of circularly polarized Alfvén waves including dispersion, J. Geophys. Res. **91**, 5617 (1986).

[10] M. Longtin and B. U. Ö. Sonnerup, Modulation instability of circularly polarized Alfvén waves, J. Geophys. Res. **91**, 6816 (1986).

[11] J. V. Hollweg, R. Esser, and V. Jayanti, Modulational and decay instabilities of Alfvén waves: Effects of streaming He + +, J. Geophys. Res. **98**, 3491 (1993).

[12] J. V. Hollweg, Beat, modulational, and decay instabilities of a circularly polarized Alfvén wave, J. Geophys. Res. **99**, 23431 (1994).

[13] Y. M. Voitenko, Three-wave coupling and parametric decay of kinetic Alfvén waves, J. Plasma Phys. **60**, 497 (1998).

[14] F. Pruneti and M. Velli, Parametric decay of large amplitude Alfven waves in the solar atmosphere, in *Fifth SOHO Workshop: The Corona and Solar Wind Near Minimum Activity*, ESA Special Publication Vol. 404, edited by A. Wilson (European Space Agency, Noordwijk, 1997), p. 623.

[15] M. Hahn, X. Fu, and D. W. Savin, Evidence for parametric decay instability in the lower solar atmosphere, Astrophys. J. **933**, 52 (2022).

[16] J. A. Klimchuk, On solving the coronal heating problem, Sol. Phys. **234**, 41 (2006).

[17] L. D. Zanna, M. Velli, and P. Londrillo, Parametric decay of circularly polarized Alfvén waves: Multidimensional simulations in periodic and open domains, Astron. Astrophys. **367**, 705 (2001).

[18] T. A. Bowen, S. Badman, P. Hellinger, and S. D. Bale, Density fluctuations in the solar wind driven by Alfvén wave parametric decay, Astrophys. J. Lett. **854**, L33 (2018).

[19] S. R. Spangler, J. A. Leckband, and I. H. Cairns, Observations of the parametric decay instability of nonlinear magnetohydrodynamic waves, Phys. Plasmas **4**, 846 (1997).

[20] Y. Narita, K. H. Glassmeier, M. Fränz, Y. Nariyuki, and T. Hada, Observations of linear and nonlinear processes in the foreshock wave evolution, Nonlinear Processes Geophys. **14**, 361 (2007).

[21] S. Dorfman, H. Hietala, P. Astfalk, and V. Angelopoulos, Growth rate measurement of ULF waves in the ion foreshock, Geophys. Res. Lett. **44**, 2120 (2017).

[22] D. Leneman, W. Gekelman, and J. Maggs, Laboratory observations of shear Alfvén waves launched from a small source, Phys. Rev. Lett. **82**, 2673 (1999).

[23] W. Gekelman, S. Vincena, N. Palmer, P. Pribyl, D. Leneman, C. Mitchell, and J. Maggs, Experimental measurements of the propagation of large-amplitude shear Alfvén waves, Plasma Phys. Controlled Fusion **42**, B15 (2000).

[24] S. Vincena, W. Gekelman, and J. Maggs, Shear Alfvén wave perpendicular propagation from the kinetic to the inertial regime, Phys. Rev. Lett. **93**, 105003 (2004).

[25] N. Palmer, W. Gekelman, and S. Vincena, Measurement of ion motion in a shear Alfvén wave, Phys. Plasmas **12**, 072102 (2005).

[26] T. A. Carter, B. Brugman, P. Pribyl, and W. Lybarger, Laboratory observation of a nonlinear interaction between shear Alfvén waves, Phys. Rev. Lett. **96**, 155001 (2006).

[27] D. W. Auerbach, T. A. Carter, S. Vincena, and P. Popovich, Control of gradient-driven instabilities using shear Alfvén beat waves, Phys. Rev. Lett. **105**, 135005 (2010).

[28] S. Dorfman and T. A. Carter, Nonlinear excitation of acoustic modes by large-amplitude Alfvén waves in a laboratory plasma, Phys. Rev. Lett. **110**, 195001 (2013).

[29] S. Dorfman and T. A. Carter, Non-linear Alfvén wave interaction leading to resonant excitation of an acoustic mode in the laboratory, Phys. Plasmas **22**, 055706 (2015).

[30] G. G. Howes, D. J. Drake, K. D. Nielson, T. A. Carter, C. A. Kletzing, and F. Skiff, Toward astrophysical turbulence in the laboratory, Phys. Rev. Lett. **109**, 255001 (2012).

[31] S. Dorfman and T. A. Carter, Observation of an Alfvén wave parametric instability in a laboratory plasma, Phys. Rev. Lett. **116**, 195002 (2016).

[32] F. Li, X. Fu, and S. Dorfman, Effects of wave damping and finite perpendicular scale on three-dimensional Alfvén wave parametric decay in low-beta plasmas, Phys. Plasmas **31**, 082113 (2024).

[33] F. Li, S. Dorfman, and X. Fu, Measuring the growth of Alfvén wave parametric decay instability using counter-propagating waves: Theory and simulations, Phys. Rev. E **112**, 025206 (2025).

[34] Y. Qian, W. Gekelman, P. Pribyl, T. Sketchley, S. Tripathi, Z. Lucky, M. Drandell, S. Vincena, T. Look, P. Travis, T. Carter, G. Wan, M. Cattelan, G. Sabiston, A. Ottaviano, and R. Wirz, Design of the Lanthanum hexaboride based plasma source for the large plasma device at UCLA, Rev. Sci. Instrum. **94**, 085104 (2023).

[35] W. Gekelman, P. Pribyl, Z. Lucky, M. Drandell, D. Leneman, J. Maggs, S. Vincena, B. Van Compernolle, S. K. P. Tripathi, G. Morales, T. A. Carter, Y. Wang, and T. DeHaas, The upgraded Large Plasma Device, a machine for studying frontier basic plasma physics, Rev. Sci. Instrum. **87**, 025105 (2016).

[36] A. Gigliotti, W. Gekelman, P. Pribyl, S. Vincena, A. Karavaev, X. Shao, A. S. Sharma, and D. Papadopoulos, Generation of polarized shear Alfvén waves by a rotating magnetic field source, Phys. Plasmas **16**, 092106 (2009).

[37] G. J. Morales and J. E. Maggs, Structure of kinetic Alfvén waves with small transverse scale length, Phys. Plasmas **4**, 4118 (1997).

[38] D. J. Thuecks, C. A. Kletzing, F. Skiff, S. R. Bounds, and S. Vincena, Tests of collision operators using laboratory measurements of shear Alfvén wave dispersion and damping, Phys. Plasmas **16**, 052110 (2009).
[39] K. D. Nielson, G. G. Howes, T. Tatsuno, R. Numata, and W. Dorland, Numerical modeling of Large Plasma Device Alfvén wave experiments using AstroGK, Phys. Plasmas **17**, 022105 (2010).
[40] S. Bose, T. Carter, M. Hahn, S. Tripathi, S. Vincena, and D. W. Savin, Measured reduction in Alfvén wave energy propagating through longitudinal gradients scaled to match solar coronal holes, Astrophys. J. **882**, 183 (2019).
[41] See Supplemental Material at http://link.aps.org/supplemental/10.1103/qc7s-scbk for additional figures.
[42] J. Barata and C. Conde, Elastic He+ on He collision cross-sections and Monte Carlo calculation of the transport coefficients of He+ ions in gaseous helium, Nucl. Instrum. Methods Phys. Res., Sect. A **619**, 21 (2010).
[43] P. Swaczyna, F. Rahmanifard, E. J. Zirnstein, D. J. McComas, and J. Heerikhuisen, Slowdown and heating of interstellar neutral helium by elastic collisions beyond the heliopause, Astrophys. J. Lett. **911**, L36 (2021).
[44] J. L. Ballester, I. Alexeev, M. Collados, T. Downes, R. F. Pfaff, H. Gilbert, M. Khodachenko, E. Khomenko, I. F. Shaikhislamov, R. Soler, E. Vázquez-Semadeni, and T. Zaqarashvili, Partially ionized plasmas in astrophysics, Space Sci. Rev. **214**, 58 (2018).
[45] H. K. Andersen, N. D'Angelo, V. O. Jensen, P. Michelsen, and P. Nielsen, Effects of ion-atom collisions on the propagation and damping of ion-acoustic waves, Phys. Fluids **11**, 1177 (1968).
[46] W. Gekelman, S. Vincena, D. Leneman, and J. Maggs, Laboratory experiments on shear Alfvén waves and their relationship to space plasmas, J. Geophys. Res. **102**, 7225 (1997).
[47] J. V. Hollweg, Kinetic Alfvén wave revisited, J. Geophys. Res. **104**, 14811 (1999).
[48] K. Nishikawa, Parametric excitation of coupled waves I. General formulation, J. Phys. Soc. Jpn. **24**, 916 (1968).
[49] M. Porkolab, Parametric processes in magnetically confined CTR plasmas, Nucl. Fusion **18**, 367 (1978).
[50] A. S. Chirkin, V. V. Volkov, G. D. Laptev, and E. Y. Morozov, Consecutive three-wave interactions in nonlinear optics of periodically inhomogeneous media, Quantum Electron. **30**, 847 (2000).
[51] L. G. Wright, F. O. Wu, D. N. Christodoulides, and F. W. Wise, Physics of highly multimode nonlinear optical systems, Nat. Phys. **18**, 1018 (2022).
[52] T. P. McKenna, H. S. Stokowski, V. Ansari, J. Mishra, M. Jankowski, C. J. Sarabalis, J. F. Herrmann, C. Langrock, M. M. Fejer, and A. H. Safavi-Naeini, Ultra-low-power second-order nonlinear optics on a chip, Nat. Commun. **13**, 4532 (2022).
[53] L. Ledezma, R. Sekine, Q. Guo, R. Nehra, S. Jahani, and A. Marandi, Intense optical parametric amplification in dispersion-engineered nanophotonic lithium niobate waveguides, Optica **9**, 303 (2022).
[54] U. Kadri and M. Stiassnie, Generation of an acoustic-gravity wave by two gravity waves, and their subsequent mutual interaction, J. Fluid Mech. **735**, R6 (2013).
[55] S. Dorfman, Replication Data for: Measurement of the Alfvén wave parametric decay instability growth rate, UCLA Dataverse, V1 10.25346/S6IQQ5ZZ (2026).
[56] A. I. Vistnes, Skin depth and waveguides, in *Physics of Oscillations and Waves: With Use of Matlab and Python*, edited by A. I. Vistnes (Springer International Publishing, Cham, 2018), pp. 553–570.

End Matter

Appendix: Pump effect on seed antenna coupling—The presence of the pump wave affects the seed antenna coupling (i.e., how wave amplitude is related to the antenna current), and we need to account for this in order to isolate the effect of PDI growth. To obtain an indicator of how well the antenna couples to the plasma, we extrapolate the field at the seed antenna ($z = z_{\mathrm{ant}} = 8.95$ m) from the exponential fit of the far-field wave amplitude profiles [Fig. 1(c)]. Results are plotted in Fig. 2(b). Because of the resonant circuit used to drive the seed antenna, the antenna current is not constant as a function of frequency; therefore, the magnetic field at $z = z_{\mathrm{ant}}$ must be scaled to the value expected for a fixed antenna current. We have confirmed the validity of this adjustment by verifying that at a fixed frequency the coupling is not a function of the antenna current (Fig. S1 in Supplemental Material [41]). Results in Fig. 2(b) show that the antenna coupling is slightly better (higher wave amplitude for the same antenna current) with the pump on; this could be related to a modification of the plasma parameters by the large-amplitude pump. To account for the difference in antenna coupling between the pump-on and pump-off cases (which has nothing to do with PDI growth), we take a ratio of the red stars and green circles in Fig. 2(b) and average over the frequency range 148–158 kHz. This choice avoids the frequency range in which seed wave damping is affected by the presence of the pump and [as discussed after Eq. (2) in the main text] the exponential fit may be unreliable. This results in an estimated $3.9 \pm 3.5\%$ enhancement in the seed wave antenna coupling with the pump on, which we account for in our PDI growth rate calculation in the main text of the Letter. The large error bar on this antenna coupling adjustment accounts for approximately 44%, 56%, and 68% of the error bar in Figs. 4(a)–4(c), respectively.

Results in Fig. 2(b) show a linear trend to lowest order, in which the antenna couples better to the plasma at higher frequency. Because the antenna is an inductive element, the

antenna loop voltage will be proportional to both frequency and antenna current, with a smaller contribution from radiation resistance. A higher antenna loop voltage means a larger oscillating electric field; the latter may accelerate electrons parallel to the mean magnetic field and help drive the wave [36]. However, the scaling shown in Fig. 2(b) is steeper than what would be expected from the model of a simple inductor, as evidenced by the fact that an extrapolation will yield a negative y intercept. For purposes of probing the PDI growth rate, we account for this trend by normalizing pump-on data to pump-off data; thus, a detailed physical explanation of the linear trend is not needed for and is beyond the scope of the present Letter. Possible ideas to explore in future work include skin depth effects in the antenna [56] and the mutual inductance between the antenna and the plasma.